PERGAMON

Journal of Structural Geology 21 (1999) 55–66

JOURNAL OF STRUCTURAL GEOLOGY

Implications of meso-structures for deformational history of the Moose Mountain structure, Canadian Rocky Mountain foothills

S. Feinstein [a], Y. Eyal [a], J.S. Bell [b]

[a] *Department of Geological and Environmental Sciences, Ben Gurion University of the Negev, Beer Sheva 84105, Israel*
[b] *Energy and Environment Subdivision, Geological Survey of Canada (Calgary), 3303-33rd Street, Calgary, Alberta T2L 2A7, Canada*

Received 13 February 1997; accepted 4 August 1998

Abstract

We use small-scale structures (meso-structures) to investigate strain and to interpret the deformation history of the Moose Mountain structure in the southern Canadian Rocky Mountains. Small-scale structures measured at seven sites encompass 440 measurements of fault planes with striations, veins and fold axes. Kinematic analysis suggests that these meso-structures record three different shortening directions that changed during the evolution of the Moose Mountain structure from NE–SW–ENE–WSW, to E–W and subsequently to NNE–SSW. NE–SW–ENE–WSW shortening is compatible with the large-scale geometry of the Moose Mountain structure and with thrust-fault orientation in the study region, whereas the relationship with E–W and NNE–SSW shortening is less obvious. Small-scale reverse faults and part of the veins are interpreted as forming during early deformation in association with the development of the macro-scale thrust faults of the Rocky Mountains, whereas the mesoscopic strike-slip faults, veins and micro-folds developed later. A relatively large number of the strike-slip faults and veins are interpreted to have been generated by reactivation of pre-existing structures. This study demonstrates again that small-scale structures can discriminate modifications in regional strain directions and identify moderate episodes of deformation within deformed terrains such as the Foothills thrust-belt.

1. Introduction

The Moose Mountain structure is located 50 km west-southwest of Calgary in the westernmost part of the Rocky Mountain foothills, Canada (Fig. 1). It is situated immediately east of the McConnell Thrust, which defines the eastern limit of the Front Ranges of the Rocky Mountains (Fig. 1). The structure consists of an upper folded and faulted thrust sheets comprising Paleozoic and Mesozoic rocks (Fig. 2) carried by the Moose Mountain Thrust Fault (Newson and Sanderson, 1996). This thrust sheet is folded over an underlying antiformal stack of thrust sheets (Fig. 2) and the whole complex has been displaced east-northeastward for several tens of kilometres (Price and Mountjoy, 1970; McMechan, 1995; Newson and Sanderson, 1996). The structure was generated in Late Cretaceous–Early Tertiary time during the Laramide Orogeny and was subsequently affected by post-orogenic uplift in the late Cenozoic (Price and Mountjoy, 1970). Like many such structures in the foothills, the axis of the Moose Mountain structure trends northnorthwest, parallel to the surface traces of associated and adjacent faults (Fig. 1). Exploration and production wells drilled on the structure have shown that what appears to be a relatively simple faulted anticline at the surface is actually a complexly-faulted anticline, cored and uplifted by an imbricate stack of thrust sheets with an east-northeast vergence (Fig. 2) (Jones, 1971; Newson and Sanderson, 1996).

The major features of Moose Mountain structure and the surrounding foothills reflect the large-scale effects of Laramide deformation in the Canadian Cordillera (Figs. 1 and 2). Nevertheless, its deformation history may involve other, possibly more moderate, regional phases of deformation that are not easily distinguished by analyses of large-scale structures. Meso-structures are features at the scale of an outcrop or smaller (mm to several m) (Hancock and Atyia, 1979; Eyal and Reches, 1983). Formation of primary and/or reactivation of pre-existing meso-structures may develop under moderate strain conditions insufficient to form new and/or reactivate older macro-structures (Eyal and Reches, 1983). In addition, rocks often retain

0191-8141/99 $ - see front matter
PII: S0191-8141(98)00090-X

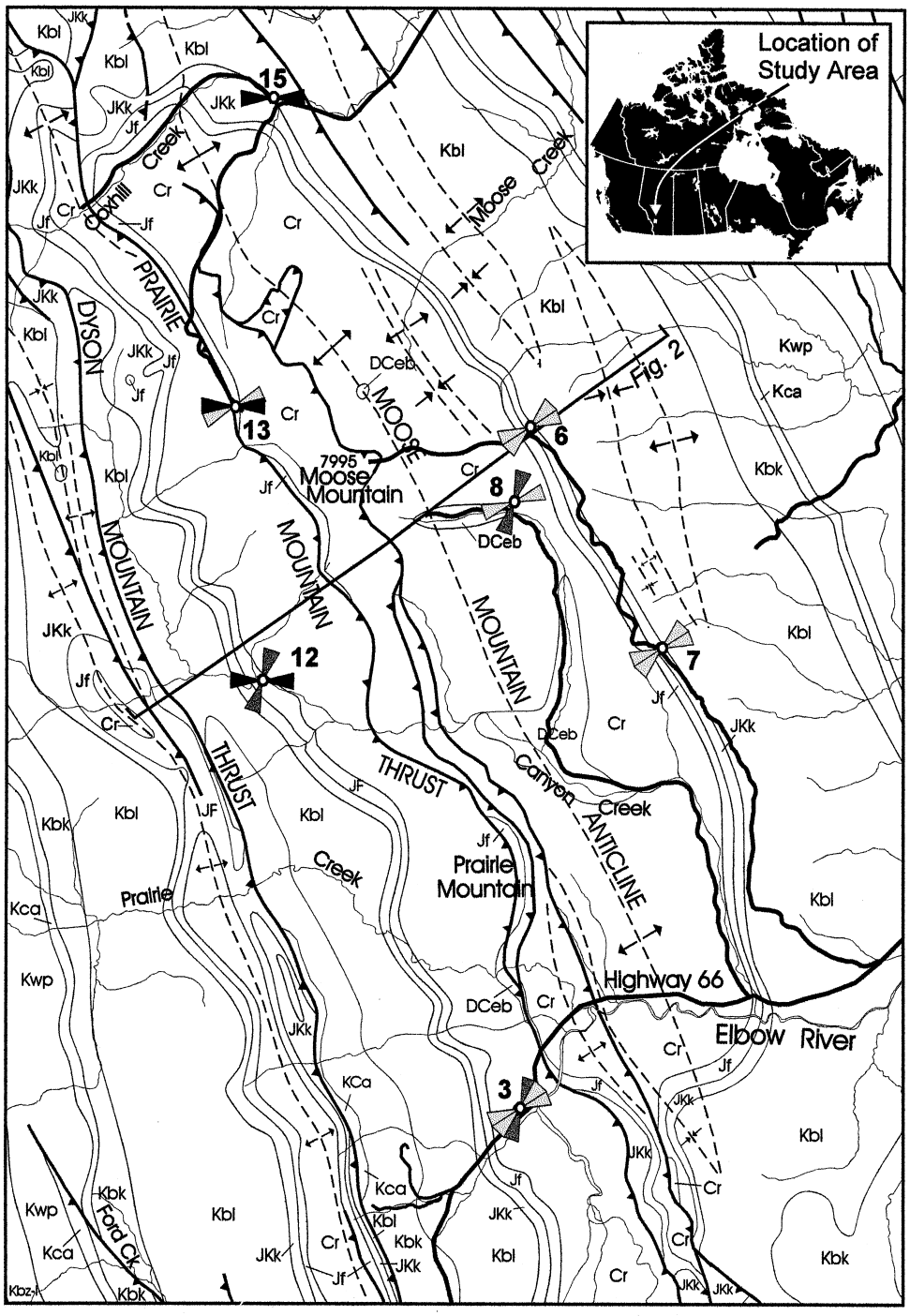

Fig. 1. Geological map of the Moose Mountain structure (after McMechan, 1995) showing locations of seven sites where meso-structures were measured. Geological symbols which correspond to those on GSC Map 1865a (McMechan, 1995) are as follows: Kbz-u—Upper part, Brazeau Formation, Kbz-l—Lower part, Brazeau Formation, Kwp—Wapiabi Formation, Kca—Cardium Formation, Kbk—Blackstone Formation, Kbl—Cadomin, Gladstone, Beaver Mines and Mill Creek Formations (undivided), JKk—Kootenay Group, Jf—Fernie Formation, Cr—Rundle Group, DCeb—Exshaw and Banff Formations. K—Cretaceous, J—Jurassic, C—Carboniferous, D—Devonian. Rose diagrams summarize shortening directions recorded at each site.

early generations of meso-structures throughout subsequent phases of deformation. In most cases, identification of reactivated meso-structures (e.g. superposition of cross-cutting sets of striations on the same fault plane) is more feasible and more precise than distinguishing reactivation of macro-structures. As an example, in the Rocky Mountains south of the study region mesoscopic subfabrics of rocks record both northerly and northwesterly trending shortening axes whereas megascopic scale structures have either

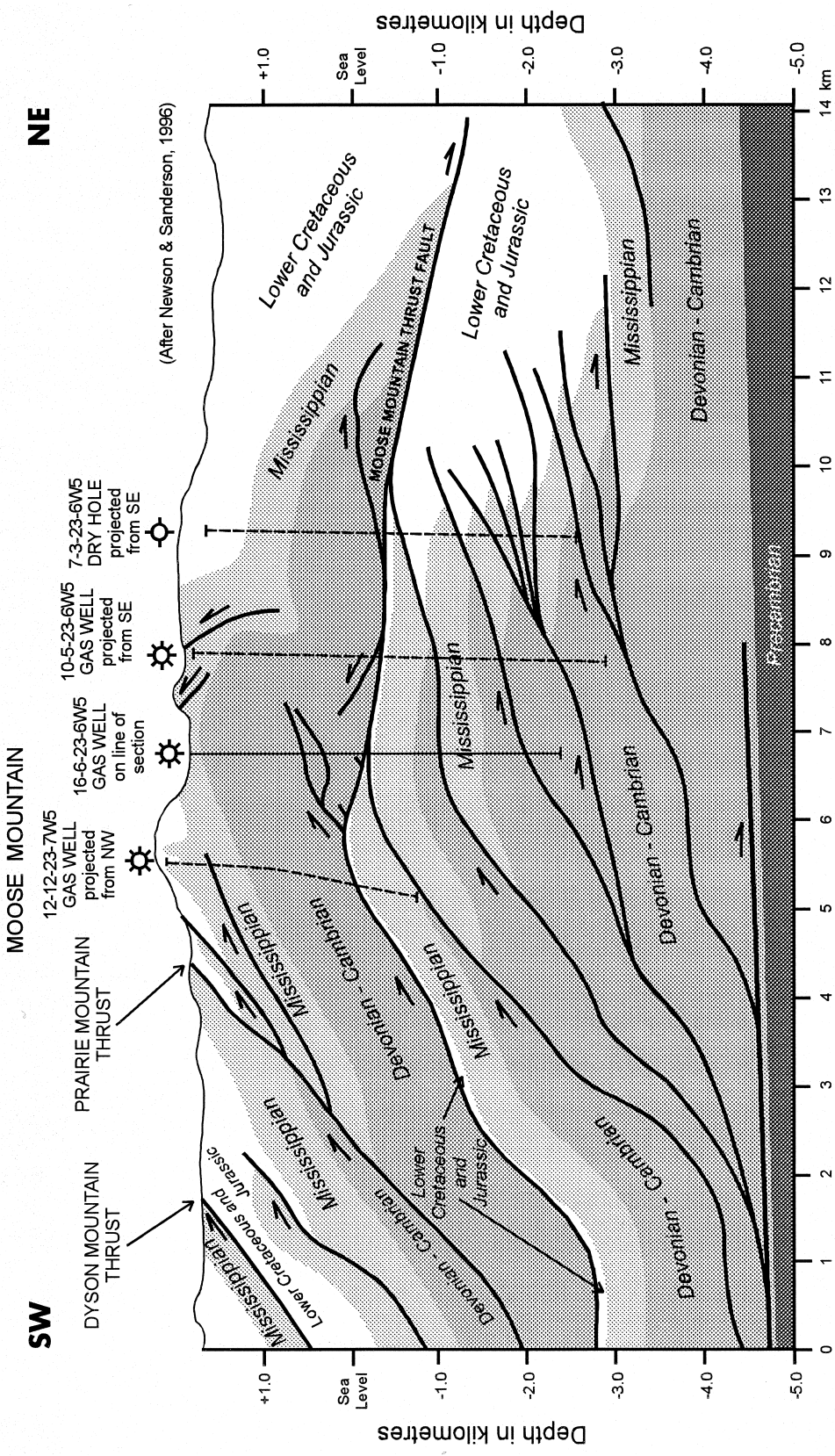

Fig. 2. Cross-section through the Moose Mountain Structure (after Newson and Sanderson, 1996). White units are Mesozoic, light gray units are Mississippian, medium gray units are Devonian to Cambrian and the dark gray legend corresponds to Precambrian basement. Location of cross-section is shown on Fig. 1.

the first trend or the second, but not both (Price, 1967). Therefore, meso-structures can often provide a more sensitive and comprehensive record of deformation history than large-scale structures, particularly for moderate strain fields and complex deformation histories. This viewpoint is at variance with conventional assertion that strain trends recorded by both macro-structures and meso-structures in the same area will essentially be consistently aligned (e.g. Wartolowska, 1972; Hancock and Atyia, 1979; Reches et al., 1981).

Price (1967) studied meso-scale structures in the southern Rocky Mountains near the Crowsnest Pass area, south of the study region. He suggests that a great number of the meso-scale structures evolved by reactivation of pre-existing fractures which were generated prior to the major thrusting. Price (1967) further indicates that movement parallel with macro-scale structures is also dominant among the meso-scale structures, but in addition, the meso-scale structures record movement along additional axes. To date, no comparable small-scale structure studies were carried out in the foothills in the Moose Mountain region. In the present study we use small-scale structures to investigate the deformation history of the Moose Mountain structure in an attempt to document changes in paleostress orientations in the deformed belt of western Canada.

2. Field measurements and data processing

The sites studied are located at a variety of stratigraphic levels and their spatial and vertical distributions provide good three dimensional cover of the upper part of the Moose Mountain structure (Fig. 1 and Table 1). We measured attitudes of meso-faults, striations on fault planes, veins and fold axes. These features comprise most of the meso-structures in the study area. General reviews of the data acquisition and analytical techniques used in this study are presented by Angelier (1979), Angelier et al. (1985), Eyal and Reches (1983), Eyal and Ron (1995) and Angelier (1994).

Maximum and minimum horizontal shortening and paleostress directions, respectively referred to as S_{Hmax} and S_{hmin}, were inferred for each locality from the strain expressed by the meso-structures mean orientations (Angelier, 1979, 1994) (Figs. 3–5). We assume that S_{Hmax} is sub-parallel to the maximum horizontal shortening axis and that S_{hmin} is aligned with the axis of maximum extension. Fold axes and veins provide indication for shortening and extension directions. The first trend is assumed to be perpendicular to, and the latter parallel to, the axes of maximum shortening. However, determination of the shortening direction from faults can be more complex. Striae on fracture surfaces are assumed to represent evidence for displacement with their plunge indicating the general trend of motion, thus allowing their classification into dip-slip and strike-slip faults. The true sense of displacement was determined in the field from relationships between secondary mineralization in small pull-apart cavities, slickolites along the striae and fault-plane irregularities. For strike-slip faults with a known sense of motion we assume that S_{Hmax} is sub-parallel to the acute bisectrix between a conjugate set of right- and left-lateral faults, or is oriented at 30° to a fault strike where the inferred sense is consistent with the observed slip. For dip-slip faults, we assume that the S_{Hmax} or S_{hmin} is perpendicular to the fault strike and depends on whether the fault is, respectively, normal or reverse. Faults for which the true sense of displacement could not be determined were assigned to either of the groups with offsets assigned on the basis of similarity of both strike and striation orientations. The assignments were made on the assumption that faults with similar attitudes would have experienced displacement in the same strain fields (for more details see Discussion).

Meso-structures studied, particularly faults, may be the product of multiple phases of deformation and reactivation of older structures. Indeed, determination of these phases and their relative timing is crucial for structural analysis of any deformed area. However, in many cases, the striae observed on a fault surface reflect mainly the later phases of deformation whereas signals for older phases may be obscured or completely erased. Hence, how far back generations of deformation can be reconstructed is restricted by the preservation of evidence.

We use Allmendinger's (1992) stereonet program for data processing and for the mean vector calculations on which the paleostrain trend determinations are based. All data were corrected (flattened) to eliminate bedding tilt at the measuring sites and the results were compared and tested for internal consistency, as discussed below.

Four hundred and forty meso-structures measured in seven sites across the Moose Mountain structure are used in this study (Fig. 1). This dataset includes 347 small faults ranging in size between a few centimetres to a few tens of metres, 51 fold axes up to a few tens of centimetres in size, and 42 calcite-filled veins. The 42 measured calcite veins comprise a small representative part only of the veins present in the sites studied. The meso-structures recorded were classified into groups based on type and orientation of structures, and their sense of motion. A total of 25 groups and their inferred S_{Hmax} were obtained for the seven sites studied. Site stratigraphy, data obtained and their classification are summarized in Figs. 3–5 and Table 1. The sense of slip along fault planes was determined in

Table 1
Data summary for meso-structure measurements. The columns from left to right are: Site number; N/n—total vs used number of fault measurements; Groups of various structures within a site; Number of measurements obtained for each group; Type of structure of each group; Mean dip and dip-azimuth of fault or vein planes; Mean plunge of striae or fold axes; $\alpha 95$–95% confidence level; Estimated S_{Hmax}; Rock units and age. ()—number of measurements and/or $\alpha 95$ value for striation. []—data for faults whose sense of motion was determined in the field

Site ♯	N/n	Figure	Group	No. of meas.	Structure type	Mean dip (dip/azimuth)	Mean plunge striae or folds	$\alpha 95$	Estimated S_{Hmax}	Rock unit and Age
3		3a	I	29 [12]	left-lateral	88/326 [88/149]	17/052 (22)	8 [9] (12)	N26°	
		3b	II	16 [4]	right-lateral	87/313	46/048 (16)	8 (24)	N73°	
			III	9 [8]	reverse-fault	81/249 [81/253]		11 [13]	N69°	
	107/77	3c					79/242 (9)	(7)		
			IV	11 [2]	reverse-fault	70/068		10	N68°	Rundle Group
							70/080 (11)	(13)		Carboniferous
			V	4 [2]	normal-fault	73/326		20	N56	
		3 d								
			VI	8 [5]	normal-fault	68/150		22	N60	
		3e	VII	11	veins	83/232		5	N142°	
Beds dip 28/256		3f	VIII	5	veins	82/313		15	N43°	
6		3 g	I	21 [4]	left-lateral	88/355		10	N55°	
		3 h	II	26 [4]	right-lateral	83/297		9	N57°	
	65/61									Kootenay Group
		3i	III	6 [1]	reverse-fault	79/049		15	N49°	Jurassic–E. Cret.
Beds dip 44/055			IV	8 [2]	reverse-fault	70/234		9	N54°	
7	37/30	3j	I	30 [7]	reverse-fault	67/227 [74/228]		7 [18]	N47°	
							59/256 (20)	(9)	(N76°)	Kootenay Group
Beds dip 29/075		3k	II	18	folds		14/165	9	N75°	Jurassic–E. Cret.
8			I	21 [10]	left-lateral	78/152 [81/155]		9 [13]		
	47/38	3 l					16/236 (21)	(12)	N16°	Exshaw/Banff
			II	17 [10]	right-lateral	41/061 [38/071]		10 [13]		Fm
Beds							12/347 (17)	(9)		Devonian
dip 28/044		3 m	III	26	veins	86/331		7	N61°	
12	22/17	3n	I	17 [7]	right-lateral	88/160 [88/164]		13 [22]	N100°	
Beds							26/066 (17)	(15)		Fernie Fm
dip 51/240		3o	II	33	folds			6	N26°	Jurassic
13			I	20 [9]	left-lateral	72/205 [68/201]	08/116 (33)	11 [20]		
		3p					2/115 (15)		N92°	
	69/69						6/074 (17)			Fernie Fm
			III	11 [5]	reverse-fault	63/066 [64/061]		18 [34]	N66°	Jurassic
Beds		3q					42/067 (8)	(13)		
dip			IV	21 [12]	reverse-fault	48/247 [41/257]		13 [19]	N67°	
38/238						83/016[84/013]	47/241 (20)	(15)		
15			I	34 [17]	left-lateral	48/247 [41/257]		6[10]		
Beds	67/52	3r					11/104 (34)	(10)	N92°	Kootenay Group
dip			II	18 [5]	right-lateral	83/169 [83/168]		6 [15]		Jurassic–E. Cret.
32/018							14/082 (18)	(9)		

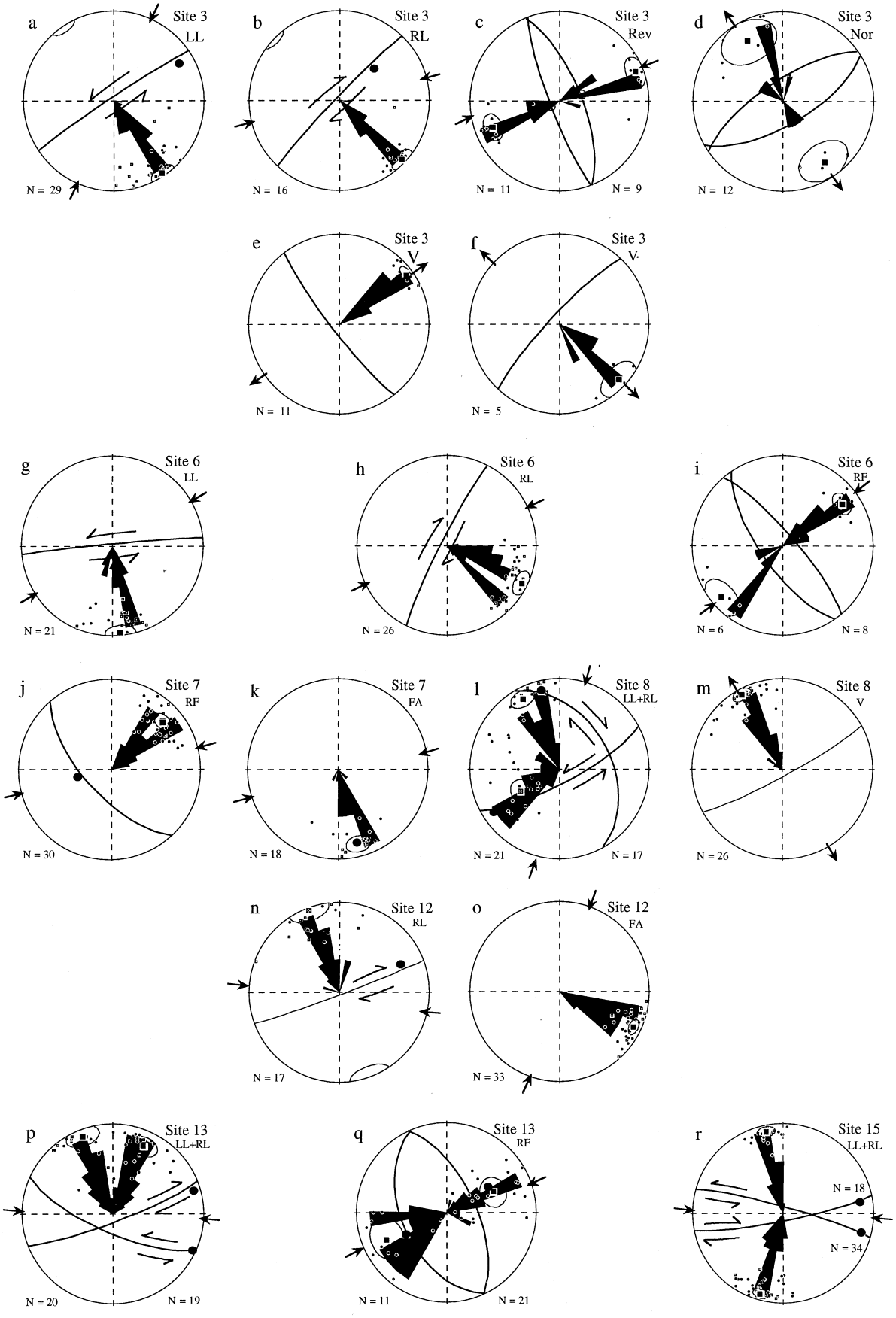

Fig. 3. Lower hemisphere equal-area stereographic projection of data for the seven sites studied. Dots and open squares represent poles to fault planes and veins, and fold axes orientations. The open squares are the upper hemisphere projection of pole to planes dipping opposite to the majority of the group. The large black squares and circles represent calculated mean pole to planes and striae, respectively. The great circle is the mean fault plane and the small circles outline 95% confidence level ($\alpha 95$). LL = left lateral; RL = right lateral; RF = reverse fault; Nor = normal fault; FA = fold axes; V = veins; large arrows indicate mean shortening and extension directions.

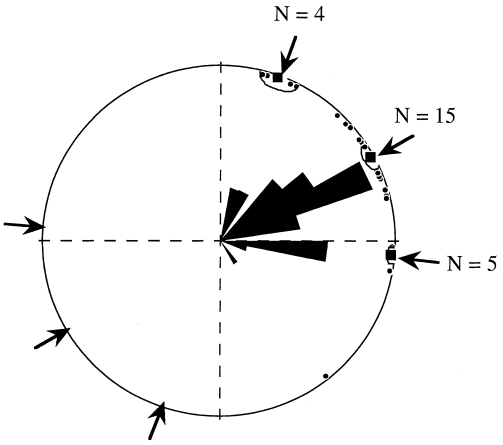

Fig. 4. Summary of shortening orientations recorded by meso-structures (lower hemisphere projection). Symbols as in Fig. 3.

the field for 38% of the faults measured (37 right-lateral, 52 left-lateral, 37 reverse faults, and seven normal faults). The rest of the faults were assigned to specific groups based on type of structure and orientation only (see Discussion). Table 1 presents the mean attitudes for an entire fault set and the mean attitudes of those faults where the sense of motion was determined in the field (13 out of 20 fault-sets include at least five such faults). The greatest difference in dip magnitudes or directions between these two categories is 10°, whereas in the majority of cases it is less than 5°.

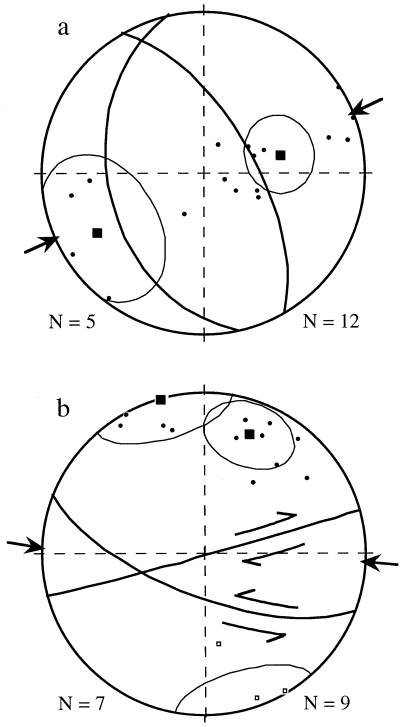

Fig. 5. Lower hemisphere equal-area stereographic projection of fault data from Site 13 whose sense of motion was determined in the field: a—reverse faults, and b—strike-slip faults. Symbols as in Fig. 3.

3. Site observations and related shortening directions

Site 3 is a roadcut within the Paleozoic Rundle Group carbonate rocks on the southwest flank of the Moose Mountain structure (Fig. 1). The meso-structures recorded at this site form eight groups (Table 1 and Fig. 3a–f). Groups I and II comprise 29 left-lateral and 16 right-lateral steeply dipping strike-slip faults (Fig. 3a and b). Both sets strike NE–SW to ENE–WSW. The mean striations are sub-horizontal and oblique and are compatible with NNE–SSW and ENE–WSW shortening, respectively. Along eight faults we found both right-lateral and left-lateral striae on the same fault plane. Groups III and IV consist of 20 high-angle reverse faults with a common strike (NNW–SSE), but opposite dips (Fig. 3c). Dip-slip striae characterizing the reverse fault planes indicate ENE–WSW shortening subparallel to that inferred for the right-lateral faults (Fig. 3b). Groups V and VI consist of 12 normal faults with a common strike (NE–SW) and around 70° dip, but in opposite directions (Fig. 3d). Some of the dip-slip striae on normal fault planes are partly overprinted by left-lateral striae. Groups VII and VIII comprise two sets of veins striking NW–SE and NE–SW (Fig. 3e and f). On some of the NE–SW veins we observed sub-horizontal striae.

Site 6 is a ridge of coarse-grained cross-bedded Jurassic Kootenay Group sandstone on the northeast flank of the structure (Fig. 1). Meso-structures measured in this site are classified into four groups (Table 1 and Fig. 3g–i). Groups I and II comprise two sets of 21 left-lateral (Fig. 3g) and 26 right-lateral (Fig. 3h) steeply dipping strike-slip faults, which are interpreted as a conjugate set. Groups III and IV consist of 14 reverse fault sets striking NW–SE to WNW–ESE, but dipping in opposite directions (Fig. 3i). The bisectrix of the acute angle of the conjugate strike-slip fault set is oriented between ENE–WSW and NE–SW. This axis coincides with a trend perpendicular to the mean strike of the reverse faults. At Site 6, the $\alpha 95$ of all the fault sets is relatively low, but their striae are highly scattered and for this reason their mean values were not included in Table 1 and Fig. 3g and h. No obvious reason for this scatter is apparent in outcrop, but it may reflect depositional fabrics of the sandstone.

Site 7 is located along a roadcut exposing Jurassic Kootenay Group clastics on the eastern flank of the Moose Mountain Structure (Fig. 1). The meso-structures studied in this site form two groups (Table 1 and Fig. 3j and k). Group I consists of 30 reverse faults (Fig. 3j) with a 67°/227° mean fault-plane dip and 59°/256° mean striations plunge (Fig. 3j) indicating slightly oblique displacements. On two of the fault planes we observed dip-slip reverse striae overprinted by right-slip striae. Group II comprises 18 small-scale fold axes obtained in sandstone, shale and coal interlayers at

this site with a 14°/165° mean plunge and azimuth (Fig. 3k). Furthermore, we observed that a few of the fault planes and their associated striae were also folded. The mean plunge of the axes of the small folds is also 14°/165°, sub-parallel to the traces of thrust faults and the axes of the larger mapped folds (Fig. 1). The axis perpendicular to the mean fold axis, assumed to correspond to the shortening direction, is parallel to the mean striae orientation of the reverse faults, implying activation under a similar stress field.

Site 8 is located on the north branch of Canyon Creek where Middle Paleozoic carbonates are exposed in the core of Moose Mountain structure. The meso-structures measured at this site classify into three groups (Table 1 and Fig. 3l and m). Groups I and II comprise 21 left-lateral and 17 right-lateral strike-slip faults (Fig. 3l). The left-lateral strike-slip faults are characterized by steep attitude (mean dip 78°/152°) and are concordant in their geometry with the 26 calcite-filled veins (cf. Fig. 3l and m). Eight of the left-lateral fault striae were measured on calcite veins. Dips characterizing the right-lateral faults are more moderate (41°/061°). Group III consists of 26 veins (with no indications of strike-slip displacement) (Fig. 3m). The veins are characterized by relatively steep dips (86°/331°). The large dihedral angle, about 90°, between the left- and right-lateral faults as well as the difference in their dips suggest that they might not have been generated as a conjugate set although they are both compatible with a NNE–SSW shortening (Fig. 3l). The mean plunge of 12°/347° recorded for right-lateral fault striae points to strike-slip movement, although the fault plane strike and moderate mean dip (41°/061°) are concordant with both the reverse faults elsewhere in the study area (e.g. Fig. 3c, i & j) and the axis of the Moose Mountain structure. The calcite-filled veins indicate NNW–SSE extension implying ENE–WSW maximum shortening (Fig. 3m). Hence, despite the concordant attitudes, the striae on the left-lateral faults record differently oriented horizontal shortening and could not have formed in the same stress field that generated the veins.

The measurements at Site 12 were made in Jurassic Fernie Formation shale and coal exposures along Canyon Creek on the southwest flank of the Moose Mountain structure (Fig. 1). The meso-structures at this site comprise two groups (Table 1 and Fig. 3n and o). Group I consists of 17 right-lateral strike-slip faults with 070° mean strike compatible of E–W shortening (Fig. 3n). Group II consists of 33 fold axes with a tightly clustered 8°/116° mean plunge that suggests NNE–SSW shortening (Fig. 3o).

Site 13 is a roadcut exposing Jurassic Fernie Formation shale and coal northwest of Moose Mountain summit. The meso-structures studied in this site form four groups (Table 1 and Fig. 3p and q). Groups I and II comprise a conjugate set of 20 WNW–ESE striking left-lateral and 19 WSW–ENE striking right-lateral strike-slip faults with acute bisectrix indicating an E–W maximum shortening axis (Fig. 3p). Groups III and IV consist of 32 reverse faults with a common NNW–SSE strike, but opposite dips (Fig. 3q). Their dip-slip striae indicate ENE–WSW shortening.

Site 15 is an outcrop of a clastic section of Jurassic Kootenay Formation on the northwestern part of the Moose Mountain anticline (Fig. 1). The meso-structures studied at this site comprise two groups of 34 left-lateral and 18 right-lateral strike-slip faults (Table 1 and Fig. 3r). These two groups form a conjugate set indicating an approximately E–W maximum shortening. Fault planes and striations were measured on two flanks of a local fold and retilting correction improves their clustering on the stereoplot suggesting that faulting predates folding (Fig. 3r). This relationship is also apparent in outcrop because the striae observed on the normal-to-bedding fault planes are bedding parallel.

4. Discussion

The measurements recorded in the seven sites studied were classified into 25 groups of meso-structures (Table 1). Assessment of the stress involved with the generation of the meso-structures may be sometimes ambiguous. Meso-structures reflect the deformation experienced at their specific locality at the time of their formation or reactivation. Whether the stress field under which the deformation recorded by a certain group of meso-structures was regional or local can be difficult to assess. Moreover, a specific assemblage of meso-structures might be developed by a variety of mechanisms and/or reactivation of pre-existing structures.

The 25 meso-structure groups recorded indicate three major shortening directions, NE–SW to ENE–WSW, E–W and NNE–SSW. The dominant shortening direction is the NE–SW to ENE–WSW which was exhibited by 15 groups from six of the seven sites, the exception being Site 12. This shortening direction is indicated by: NW–SE striking reverse faults (Sites 3, 6, 7 and 13); ENE–WSW striking left-lateral strike-slip faults (Site 6); NE–SW striking right-lateral strike-slip faults (Sites 3 and 6); NE–SW striking veins (Sites 3 and 8); NE–SW normal faults (Site 3), and SSE plunging fold axes (Site 7). E–W shortening is indicated by five groups in three sites: ENE–WSW striking right-lateral strike-slip faults (Site 12) and two conjugate sets of strike-slip faults (Sites 13 and 15). Shortening along a NNE–SSW direction is indicated by four groups from three sites: NE–SW striking left-lateral strike-slip faults (Site 3), a conjugate set of strike-slip faults (Site 8) and ESE plunging fold axes (Site 12).

From the small displacement recorded along the meso-faults and cumulative width of veins in the studied area we estimate that the total deformation involved with the meso-structures studied is about 5%. Hence, we assume a coaxiality of the principal strains and paleostresses (e.g. Reches and Eyal, 1983). This implies that the deformation history of the Moose Mountain structure according to the studied meso-structures was associated with three different paleo S_{Hmax} oriented NE–SW to ENE–WSW, E–W and NNE–SSW (Fig. 4). Of the three shortening directions, the NE–SW to ENE–WSW maximum shortening direction is anticipated since it is perpendicular to the axis of the Moose Mountain structure (Fig. 1) and to the surface traces of regional thrust faults in the area. This compression orientation is dominant among the meso-structures in the study area and is aligned with the structures of the youngest deformation phase of the Rocky Mountain Front Ranges (Ower, 1975; Price, 1981; McMechan and Thompson, 1989; Monger, 1989; McMechan, 1995). However, this is not the case with structures indicating E–W and NNE–SSW orientations of maximum shortening. The large-scale structures of the Rocky Mountains provide no obvious evidence of such stress regimes.

4.1. Grouping of meso-faults

The 20 fault groups listed in Table 1 and illustrated in Fig. 3 were assembled by combining faults, for which the sense of motion was determined by field evidence, with those for which the sense of motion was inferred based on similarity in attitudes of their planes and striae to the former. Grouping meso-faults in this way can be equivocal, particularly in tectonically complex terrains. However, the assumption that faults with similar strikes and striation trends have developed under a similar strain provides the simplest explanation. The uncertainty involved has limited significance for the study since all fault groups (Table 1 and Fig. 3) include faults for which true senses of motion were determined. False inferences would affect only the number of faults attributed to a certain group, but not the actual existence of the group or the inferred shortening direction.

For example, at Site 13 we report two groups of 39 strike-slip faults and two groups of 32 reverse faults (Table 1 and Fig. 3p and q). Striae orientations define all faults in the first groups as strike-slip and in the second as dip-slip, but cannot resolve between left- or right-lateral and normal or reverse slip. However, mineralization in small pull-apart cavities allows further determination of nine left-lateral and seven right-lateral faults within the strike-slip groups and 17 reverse displacements in the dip-slip groups (Fig. 5 and Table 1). The other 11 left-lateral, 13 right-lateral and 15 reverse faults (Fig. 3p and q, Table 1) were classified by inferrence based on similarity of faults and striae orientations. Differences are small between mean attitudes for faults whose sense of motion was defined in the field vs those for all faults (cf. Fig. 3p vs 5a and 3q vs 5b).

At Site 3 we report 45 strike-slip faults striking generally northeast (Table 1 and Fig. 3a and b). Of these, field evidence indicates that 12 are left-lateral and four are right-lateral faults (Table 1). Classification of the remaining 24 strike-slip faults by inference probably involves the greatest uncertainty of all cases in this study due to the close attitude of both strike-slip groups. Nevertheless, even if some or, in the worst case, all 14 left-lateral and 10 right-lateral faults are improperly assigned, the deviation of mean attitudes with respect to that of the 16 strike-slip faults with known senses of motion is relatively small (~3°). Moreover, the inference of ENE–WSW shortening from the right-lateral faults is augmented by the similar shortening axis implied by the reverse and normal faults in the same site (Fig. 3c and d). The NNE–SSW shortening suggested by the left-lateral faults is consistent with meso-structural evidence at several other sites (e.g. fold axis in site 12).

It should be emphasised that classification by inference applies only to faults. It is used to assign a shear sense to strike-slip faults and normal vs reverse for dip-slip faults where the striae are not sufficiently diagnostic.

4.2. Paleostrain orientation and relative timing

It is worth considering the distribution of the paleostrain indicators and their possible timing implications. Each of the three shortening orientations was recorded by a variety of structures in at least three different sites. None of the seven sites contained meso-structures recording all three shortening directions. However, five sites (3, 7, 8, 12, 13) have indications of two different shortening directions.

The youngest rock unit that contains evidence for all three shortening directions is the Jurassic Fernie Formation. This implies that all three shortening directions recorded by the meso-structures are post-Jurassic, and possibly even post-Late Cretaceous, comparable with the time suggested for the Laramide deformation. Relative timing of different shortening directions can be established in some cases based on relationships between structures. Reverse faults at Site 7 dip SW (227°) and their mean striae orientation is WSW (256°) (Fig. 3j). Reverse faults in three other sites in the study area (Sites 3, 6 and 13) are all characterised by NE–SW to ENE–WSW dip orientation and dip-slip striae (Fig. 3), indicating similar shortening. We tentatively assume that the fault planes

in Site 7 also originated as pure reverse faults under NE–SW shortening and the ENE–WSW striae represent a later, slightly oblique motion on these fault planes. This possibility is further corroborated by striae cross-cutting relationships on two of the fault planes. However, the possibility of a mixed-mode single deformation cannot be excluded. Small-scale fold axes indicating ENE–WSW shortening in Site 7 (Fig. 3k) which deform some fault planes and striae further suggest that the reverse faulting predates the folding and that shortening orientation changed from NE–SW (~045°) at an early stage to ENE–WSW (075°) later on.

At Site 8 (Fig. 3l and m and Table 1) veins striking 061° indicate extension perpendicular to this direction, whereas the left-lateral and right-lateral strike-slip faults represent NNE–SSW shortening. As noted above, the dihedral angle for the apparent conjugate set of strike-slip faults is 90°, considerably wider than the expected value of about 60°. The mean attitude of the right-lateral faults is, on one hand, characterized by a relatively low dip compared to the sub-vertical strike-slip faults elsewhere in the area, and, on the other hand, its strike is sub-parallel to that of the reverse faults at other sites (Fig. 3c, i, j and q). This correspondence in orientation suggests that the right-lateral strike-slip faults in Site 8 could have originally formed as reverse faults under an ENE–WSW shortening, similar to that recorded by the veins at this location (Fig. 3m and Table 1). If this is the case, the right-lateral slip represents reactivation of pre-existing reverse faults under NNE–SSW compression (Fig. 3l). The pre-existing zones of weakness enabled the evolution of right-lateral slip despite the deviation from an optimal shear orientation. A similar mechanism probably applies also for the left-lateral strike-slip faults in Site 8 where striae recorded on veins and almost identical mean strikes of faults and veins suggest that the left-lateral slip is due to reactivation of former extensional fractures (Fig. 3l and m). In such a case, the veins and inferred former reverse faults would have been generated by ENE–WSW shortening. Subsequently, NNE–SSW compression reactivated both pre-existing structures and produced the right and left-lateral offsets.

At Site 3 the reverse (Fig. 3c), normal (Fig. 3d), and right-lateral strike-slip faults (Fig. 3b) are consistent with an ENE–WSW shortening, whereas the northeast-striking set of veins (Fig. 3f) suggests NW–SE extension (i.e. NE–SW S_{Hmax}). The left-lateral strike-slip faults (Fig. 3a), although with a similar orientation to the right-lateral faults (Fig. 3b), indicate NNE–SSW shortening. Moreover, striae indicating both right-lateral and left-lateral displacements are present on the same fault plane. Indeed, the two opposing displacements could not have been generated under the same stress field. Unfortunately, we could not determine relative timing between the two types of striae. However, both sets of strike-slip faults have a similar orientation to the NE–SW striking vein set and the normal faults (cf. Fig. 3a, b, d and f). In both strike-slip fault sets, striae were observed on calcite veins. Some dip-slip normal striae are partly overprinted by left-lateral striae. This evidence indicates that the NE–SW veins and normal faults predate both strike-slip movements. Hence, we suggest tentatively that these relationships document three deformation phases. The NE–SW striking veins and normal faults represent the earliest deformation phase that evolved under shortening, shortening at the same orientation and perpendicular extension (Fig. 3d and f). A subsequent change to ENE–WSW shortening resulted in reactivation of the NE–SW pre-existing tensional fractures as right-lateral faults (Fig. 3b) and the formation of the reverse faults (Fig. 3c). The left-lateral strike-slip faults which record NNE–SSW shortening postdate the meso-structures formed by NE–SW shortening, but no direct evidence was found for their time relationship to meso-structures which record ENE–WSW shortening. However, at Site 8 meso-structures indicate that NNE–SSW shortening postdates the NE–SW to ENE–WSW shortening. The indication that NE–SW predates ENE–WSW shortening is consistent with the relationships recorded at Site 7.

Right and left-lateral strike-slip faults at Sites 12, 13 and 15 (Fig. 3n, p and r and Table 1) suggest E–W shortening. Unfortunately, in none of these sites could we identify clear-cut indications for relative timing of this shortening direction. However, faults measured at Site 15 on both flanks of a NNE-plunging fold cluster, after retilting, into homogenous left- and right-lateral groups (Fig. 3r). This suggests that the deformation of the meso-faults occurred at an early stage and was followed by map-scale folding with both involving similar E–W shortening.

The Moose Mountain structure developed through a complex sequence of thrusting and folding (e.g. Newson and Sanderson, 1996). Meso-scale structures could have developed at any of these deformation stages. The data observed do not provide unequivocal indication for the time of the meso-structure development relative to the macro-scale structures. As a first approximation, we assumed that they had been formed before the major macro-scale structures; hence all the data in Fig. 3 and Table 1 were calculated as though the beds were horizontal during deformation. However, meso-structures could have developed at any stage of deformation. As an example, Newson and Sanderson (1996) interpreted small back thrusts in the subsurface (Fig. 2). These thrust faults probably formed during a relatively late stage of the Moose Mountain deformation. Meso-scale reverse faults

could have developed in association with this late back thrusting. However, the improved clustering of data and derived shortening directions when plotted after retilting (Figs. 3 and 4) further supports the assumption that the meso-scale structures were formed before the major episodes of Laramide thrusting and folding.

The macro-scale structural pattern reflects in general NE–SW to ENE–WSW shortening, similar to the majority of the meso-structures, and thus could have evolved simultaneously, or at a late stage under the same general strain field. However, meso-scale structures related to NNE–SSW shortening appear to be younger than those related to NE–SW to ENE–WSW shortening and could have developed or been reactivated after the general tilting. Hence, the application of retilting correction to these structures is uncertain. However, because of the geometries involved, the differences in mean S_{Hmax} attitudes of these five groups of structures that result from a retilting range from 2° to 9°, and do not affect the results in any significant way.

The kinematic history of the Moose Mountain structure based on meso-structural analysis indicates three distinct shortening directions and related paleostress, S_{Hmax} orientations (Fig. 4). The NE–SW–ENE–WSW shortening, dominant among the meso-structures in the study area, aligns with the axis of the Moose Mountain structure (Fig. 1) and is in accordance with the youngest deformation phase of the Rocky Mountain Front Ranges (Ower, 1975; Price, 1981; McMechan and Thompson, 1989; Monger, 1989; McMechan, 1995). Clustering of meso-structural groups from both flanks of the Moose Mountain structure into E–W and NNE–SSW shortening (Fig. 4) suggests that these S_{Hmax} were effective at least at the scale of the Moose Mountain structure. However, the significance of these shortening directions for the regional kinematic and tectonic history of the Rocky Mountains is less certain.

Both E–W and NNE–WSW shortening directions are also indicated by meso-scale structures in the Front Ranges south of the study area (Price, 1967; e.g., respectively, figs 10 and 18). Furthermore, it is interesting to note that the inferred NNE–SSW compressional axis is sub-parallel to major intra-continental dextral shear zones in the Canadian Cordillera. Price and Carmichael (1986) compiled the evidence for major dextral offsets to the west and northwest of the study area along the Tintina Trench–Northern Rocky Mountain Trench fault zone and the Fraser River–Straight Creek fault zone. They suggest that most of the dextral slip on the Tintina trench–Northern Rocky Mountain trench fault zone was transformed southwards into oblique convergence in the southern Rocky Mountains during Late Cretaceous and Paleocene time. Though it is not exactly in the orientation anticipated by Price and Carmichael (1986), it is conceivable that this event represents an inboard effect of strike-slip faulting to the west in late Mesozoic–early Tertiary time. Obviously, much more wide ranging field studies are required to assess this possibility.

In the U.S. Rocky mountains to the south of the study area, NE–SW, E–W and N–S–NNE–SSW shortening orientations have been identified and attributed to the opening of the North Atlantic Ocean during Cretaceous–Tertiary time (Gries, 1983). Gries (1983) interprets that, unlike our results, shortening orientations in the northern U.S. Rocky Mountains evolved from E–W to NE–SW, but in accordance with our results she suggests that the N–S–NNE–SSW shortening is the youngest phase. She relates this latter shortening trend to the opening of the Arctic Ocean during the middle Paleocene. The similarity of the three shortening trends between these two regions raises the possibility that the meso-structures in the Moose Mountain structure have regional significance.

5. Conclusions

1. Analysis of meso-structures delineates several phases in the deformation history of the Moose Mountain structure and provides constraints on their nature and relative timing.
2. In the Moose Mountain area, we interpret earliest deformation to have involved NE–SW shortening that appears to have changed to ENE–WSW and later to E–W directed shortening.
3. We interpret the existence of a younger, less intense deformation phase that involved NNE–SSW shortening.
4. All small-scale reverse faults in the study area were probably formed during the early deformation phase in association with large-scale thrusting in the Rocky Mountains. This inference is further supported by an improved clustering on stereoplot after retilting. Some of the veins are interpreted to have formed simultaneously with the reverse faulting. On the other hand, the small-scale strike-slip faults and folds clearly are products of later deformation phases. However, some of the strike-slip faults and some of the veins were probably produced by reactivation of pre-existing structures.
5. The study further demonstrates that meso-structures can document phases of deformation which macro-structural information and regional field mapping will not readily reveal and record the internal deformation history of large thrust sheets.

Acknowledgements

The authors are grateful to Kirk Osadetz for his enthusiastic support and logistical assistance. Glen Elliott and Murray Powe of Husky Oil authorised us to use their company's well-site access roads, and Ross Mannering of the Alberta Department of Lands and Forests provided us with keys to gates of the Moose Mountain and Canyon Creek roads. The staff at the Shell Canada Gas Plant provided transportation and permitted us to make measurements close to their well-heads. All this assistance was invaluable in accelerating our fieldwork. Y. Shalmi assisted in organising the data base and preliminary processing. The manuscript has greatly benefitted from comments by K. Osadetz and G. Stockmal, and thorough review by B. A. Couzens-Schultz and R. J. Scammell.

References

Allmendinger, R.W., 1992. Stereonet 4.5 computer application program. Department of Geological Sciences, Cornell University, Ithaca, New York, U.S.A.

Angelier, J., 1979. Determination of the mean principal directions of stresses for a given fault population. Tectonophysics 56, T17–T26.

Angelier, J., 1994. Fault slip analysis and paleostress reconstruction. In: Hancock, P.L. (Ed.), Continental Deformation, pp. 53–101. Pergamon Press.

Angelier, J., Colletta, B., Anderson, E.R., 1985. Neogene paleostress changes in the Basin and Range: A case study at the Hoover Dam, Nevada-Arizona. Geological Society of America Bulletin 96, 347–361.

Eyal, Y., Reches, Z., 1983. Tectonic analysis of the Dead Sea Rift region since the Late Cretaceous based on meso-structures. Tectonics 2, 167–185.

Eyal, Y., Ron, H., 1995. Late Cenozoic crustal deformation of the north-central Basin and Range Province, Western U.S.. Tectonophysics 246, 211–224.

Gries, R., 1983 North–south compression of Rocky Mountain foreland structures. In: Lowell, J. D., Gries, R., (Eds.), Rocky Mountain Foreland Basins and Uplifts, pp. 9–32. Rocky Mountain Association of Geologists, Denver.

Hancock, P.L., Atyia, M.S., 1979. Tectonic significance of mesofractures systems associated with the Lebanese segment of the Dead Sea transform fault. Journal of Structural Geology 1, 143–153.

Jones, P.B., 1971. Folded faults and sequence of thrusting in Alberta Foothills. American Association of Petroleum Geologists Bulletin 55, 292–306.

McMechan, M.E., 1995. Geology, Rocky Mountain Foothills and Front Ranges in Kananaskis Country, Alberta. Geological Survey of Canada, Map 1865a, scale 1:100,000.

McMechan, M.E., Thompson, R. I. (1989) Structural style and history of the Rocky Mountain fold and thrust belt. In: Ricketts, B., (Ed.), Western Canada Sedimentary Basins, pp. 47–71. Canadian Society of Petroleum Geologists, Calgary.

Monger, J.W.H., 1989. Overview of Cordilleran Geology. In: Ricketts, B., (Ed.), Western Canada Sedimentary Basins, pp. 9–32. Canadian Society of Petroleum Geologists, Calgary.

Newson, A.C., Sanderson, D.A., 1996. Moose Mountain: An example of an oil and gas pool in the overthrust belt of the Canadian Rocky Mountains. Canadian Society of Petroleum Geologists Field Trip, Institute of Sedimentary and Petroleum Geology, Calgary.

Ower, J., 1975. The Moose Mountain structure, birth and death of folded fault play. In: Evers, H. J., Thorpe, J. E., (Eds.), Structural Geology of the Foothills Between Savanna Creek and Panther River, S.W. Alberta, Canada, pp. 22–29. Guidebook, Canadian Society of Petroleum Geologists and Canadian Society of Exploration Geophysicists, Calgary.

Price, R.A., 1967. The tectonic significant of mesoscopic subfabrics in the southern Rocky Mountains of Alberta and British Columbia. Canadian Journal of Earth Sciences 4, 39–70.

Price, R.A., 1981. The Cordilleran thrust and fold belt in the southern Canadian Rocky Mountains. In: McClay, K. R., Price, N. J., (Eds.), Thrust and Nappe Tectonics, Vol. 9, pp. 427–448. Geological Society of London, Special Publication.

Price, R.A., Mountjoy, E.W., 1970. Geological structure of the Canadian Rocky Mountains between Bow and Athabasca Rivers—a progress report. In: Wheeler, J. O., (Ed.), Structure of the Southern Canadian Cordillera, Vol. 6, pp. 7–25. Geological Association of Canada, Special Paper.

Price, R.A., Carmichael, D.M., 1986. Geometric test for Late Cretaceous–Paleogene intracontinental transform faulting in the Canadian Cordillera. Geology 14, 468–471.

Reches, Z., Hoexter, DF., Hirsch, F., 1981. The structure of a monocline in the Syrian Arc system, Middle East—surface and subsurface analysis. Journal of Petroleum Geology 3, 415–425.

Wartolowska, J., 1972. An example of the process of tectonic stylolitization. Bulletin of Academy Polonais Sciences 20, 197–294.